Ultrasonics 68 (2016) 89–101

Contents lists available at ScienceDirect

Ultrasonics

journal homepage: www.elsevier.com/locate/ultras

Multidimensional spectral analysis of the ultrasonic radiofrequency signal for characterization of media

Simona Granchi [a], Enrico Vannacci [a], Elena Biagi [a,*], Leonardo Masotti [b]

[a] Department of Information Engineering (DINFO), University of Florence, via Santa Marta 3, 50139 Florence, Italy
[b] El.En. S.p.A., Scientific Committee, Via Baldanzese 17, 50041 Calenzano, Florence, Italy

ARTICLE INFO

Article history:
Received 1 July 2015
Received in revised form 8 February 2016
Accepted 11 February 2016
Available online 16 February 2016

Keywords:
Ultrasonic radiofrequency signal
Spectral analysis
Signal processing
Tissue characterization
Quantitative ultrasound

ABSTRACT

The importance of the analysis of the radiofrequency signal is by now recognized in the field of tissue characterization via ultrasound. The RF signal contains a wealth of information and structural details that are usually lost in the B-Mode representation. The HyperSPACE (Hyper SPectral Analysis for Characterization in Echography) algorithm presented by the authors in previous papers for clinical applications is based on the radiofrequency ultrasonic signal. The present work describes the method in detail and evaluates its performance in a repeatable and standardized manner, by using two test objects: a commercial test object that simulates the human parenchyma, and a laboratory-made test object consisting of human blood at different dilution values. In particular, the sensitivity and specificity in discriminating different density levels were estimated. In addition, the robustness of the algorithm with respect to the signal-to-noise ratio was also evaluated.

1. Introduction

When an ultrasonic wave propagates through soft tissue, an interaction occurs between the mechanical energy of the wave and the local structure, generating energy absorption, reflection, and scattering. The energy propagated back toward the ultrasonic transducer constitutes the ultrasonic echo signal called the radiofrequency (RF) signal. The RF signal contains information about ultrasound–tissue interaction [1–8] and a processing method must be used that is capable of extracting this information.

The amplitude is related to the distribution of mechanical impedance (density, elastic characteristics) of the backscattering medium, the scatterer concentration and the ratio between the sizes of the microstructure and the wavelength [1,3,9,10]. The phase information, related to the interferences, depends on the mutual distances and geometrical organization of the tissue microstructure scatterers. These interferences and reflectivity variations in the time domain are responsible for spectral amplitude modulation in the frequency domain. In this context, over the last thirty years quantitative ultrasound (QUS) techniques have been developed [11–13] to improve tissue characterization as a support for diagnostics. Indeed, in order to gain further information for tissue characterization and differentiation purposes, it is essential not only to preserve the shape of the RF signal spectrum, but also to identify the spectral parameters that are best correlated with the investigated structures [3,4,9,14–25].

Our group used the RF signal for our investigation techniques [26,27] and developed the RULES (Radiofrequency Ultrasonic Local EStimators) algorithm [28–32] based on the analysis of the local power spectrum obtained by DWPT (Discrete Wavelet Transform). Even though significant results have been achieved in various research fields [23,27–29,33,34], they have been below expectations. In fact, the method was dependent on the instrumental parameters of the acquisition setup [24,25] and the number of extracted features was insufficient for characterizing tissue with good specificity and sensitivity as demonstrated by the results obtained by comparing the RULES with the method discussed in this paper [35].

The proposed investigation method called HyperSPACE (Hyper SPectral Analysis for Characterization in Echography) is able to extract local information about the tissue under investigation and implements a sub-band spectral decomposition. The method in not directly based on the analysis of the power spectrum of the RF signal, as with RULES and the principal QUS techniques, however it works in a spectral domain of *N*-dimensions; this is the origin of the Hyper suffix in the name, where *N* is the number of sub-bands into which the RF signal bandwidth is decomposed.

* Corresponding author at: Ultrasound and Non-Destructive Testing Lab, Department of Information Engineering (DINFO), University of Florence, via Santa Marta 3, 50139 Florence, Italy. Tel.: +39 055 2758606; fax: +39 055 2758570.
E-mail address: elena.biagi@unifi.it (E. Biagi).

http://dx.doi.org/10.1016/j.ultras.2016.02.010
0041-624X/

The method was applied in an important experimentation involving ten Italian hospital clinics in order to differentiate the two most common breast pathologies [35–37]. High values of sensitivity and specificity in differentiating fibroadenoma and infiltrating ductal carcinoma were obtained and compared with histological examinations.

In previous works, we focused our attention on the training phase of the algorithm and the description of the results. In the present paper, the fundamental steps of the algorithm are explained in detail. Moreover, the sensitivity of the method, the dependence of the method on the instrumental parameters, and the robustness of the algorithm with respect to the signal-to-noise ratio (SNR) have been estimated. To do this, it was important to test the method starting from the analysis of a single parameter by using commercial and simple test objects. Two different test objects were used. The first, a commercial CIRS model 047 (Computerized Imaging Reference Systems, Inc. Norfolk, Virginia 23513 USA) test object, consists of background material that simulates the human parenchyma with a series of aggregates at different densities inserted to simulate the presence of cysts. The second was a laboratory test object consisting of a transfusion bag containing human blood at different concentrations. Due to the characteristics of the two test objects, density was chosen as the parameter for evaluating the properties of the HyperSPACE algorithm.

2. Investigation method

The proposed algorithm can be classified as a QUS technique based on the analysis of the backscattered ultrasonic RF signal. Moreover, it performs a sort of Texture Analysis [13,38–40] as it tries to characterize the echographic image by extracting the typical features that determine the texture. In diagnostic ultrasounds, texture analysis can be performed either directly by analyzing the correlations among spatial gray-levels of B-Mode images, or indirectly with QUS techniques applied to the spectral features. The purpose of the algorithm is to identify a new spectral domain where the signal parameters, correlated with the mechanical characteristics and structural organization of the medium under investigation, can be extracted.

The investigation method works in a hyperspace consisting of N spectral dimensions obtained from a sub-band decomposition of the RF signal in order to read the local spectral amplitude modulations generated by the distribution of the scatterers. Another specific characteristic of the method is the implementation of "local normalization" that takes into account the effective energy of the ultrasonic wave which insonifies the "local" portion of the medium. In addition, the proposed normalization allows the algorithm to be independent from the instrumental acquisition parameters of the echographic scanner, such as Time Gain Compensation (TGC) and transmission power.

The HyperSPACE algorithm procedure is illustrated in Fig. 1. The processing procedure is broken down into four main phases that are explained in detail below.

2.1. Sub-band decomposition

The first step consists of the decomposition of the signal in the spectral sub-bands, while in the second, the HyperSPACE coefficients are produced. The third is a training procedure applied in order to identify sets of parameters, called Configurations, that are able to characterize the investigated medium. In the fourth phase, the RF frames are classified according to the parameters identified in the previous phase.

The HyperSPACE implements a decomposition of the spectrum by performing a convolution in the time domain between each track of the RF frame with N bandpass filters, the impulse responses $h(t)$ of which have a high degree of correlation with the echographic signal. From among the possible options, the Morlet function, widely used in literature for ultrasonic signals, was chosen as the impulse response [16,41–44]:

$$h(t) = \frac{\beta}{\sqrt{2\pi}} e^{\frac{\beta^2 t^2}{2}} \cos(\mu_k t) \tag{1}$$

In the time domain this signal represents a cosine function modulated by a Gaussian function. The parameters β and μ_k determine the time duration of the response (i.e. its spectral bandwidth) and the central frequency location of the filter respectively. These filters exhibit the same compact support in the time domain. In the spectral domain, they show a different central frequency and the same bandwidth. The bandwidth of the filters and their central frequency spacing depends on the degree of spectral resolution selected.

In this work, the RF signal was acquired with a sampling frequency of 50 MHz and a bank of 24 filters was generated by choosing a constant value of β in order to obtain a bandwidth of 1 MHz at −12 dB, the choice of which is explained in Section 4. The value of μ_k was set so that the central frequencies of the filters were multiples of 1 MHz. These 24 spectral sub-bands represent the dimensions of the domain in which the HyperSPACE analyzes the signal. The decomposition procedure of the RF signal is illustrated in Fig. 2, where it can be observed how each track of the RF frame (Fig. 2a and b) is decomposed by a filter bank. In Fig. 2c several impulse responses of the filters are shown. If Sb_1, Sb_2, …, Sb_N are the N sub-bands into which the signal spectrum is decomposed, then the RF signal at time t_0 can be represented by N coefficients c_1, c_2, …, c_N, that are the convolution coefficients between the signal and each filter of the bank as shown in Fig. 2d. In this way, it is possible to know the corresponding N coefficients in the transformed domain for any instant t_0 of the RF signal. For each RF track formed by Y samples, Y vectors of length N are obtained and consequently, C_{Sb} matrices with dimensions X by Y are derived for each frame constituted by X tracks. Each of these C_{Sb} matrices contains the coefficients, called $c_{i,m,Sb}$, relating to a particular sub-band, indicated by the subscript Sb; the other two subscripts i and m indicate the position within the matrix (and hence the track and the time instant associated with the coefficient). In our case, 24 C_{Sb} matrices are produced for each RF frame.

2.2. HyperSPACE coefficient generation

In order to increase the performance of a method it is necessary to make it as independent as possible from any amplitude variations determined by the settings of the instrumental acquisition set-up, or by the characteristics of previously encountered structures. For this reason, a distinctive feature of the proposed method consists of performing a normalization process that takes the actual ultrasonic signal into account locally, i.e. within a window of limited size, which is present in the investigated portion of the sample. This operation, which can be called "Local Normalization", is illustrated in Fig. 3, where the entire procedure of the HyperSPACE coefficient generation is shown. The first step (Fig. 3a) consists of a local average performed to reduce the variability of the coefficients. This is carried out by sliding a partially overlapped window on top of the absolute values of each of the N C_{Sb} matrices. The size of the N matrices obtained, called Local Average Matrices (LAM_{Sb}), is K by J depending on the choice of the size of the sliding window and the overlaps, according to (2):

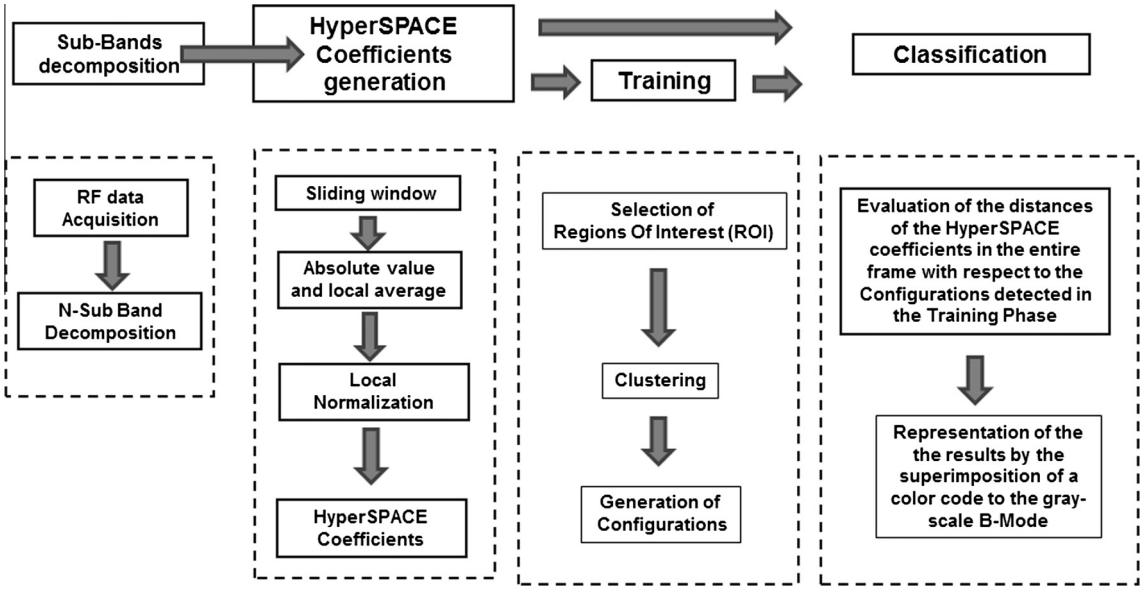

Fig. 1. HyperSPACE (Hyper SPectral Analysis for Characterization in Echography) block diagram. The first step consists of the decomposition of sub-bands for spectral coefficients extraction, the second entails the generation of the HyperSPACE coefficients. The third step is the training procedure on ROI applied on the HyperSPACE coefficients for Configuration generation. The last step is the Classification phase over the entire frame for revealing the presence of Configurations.

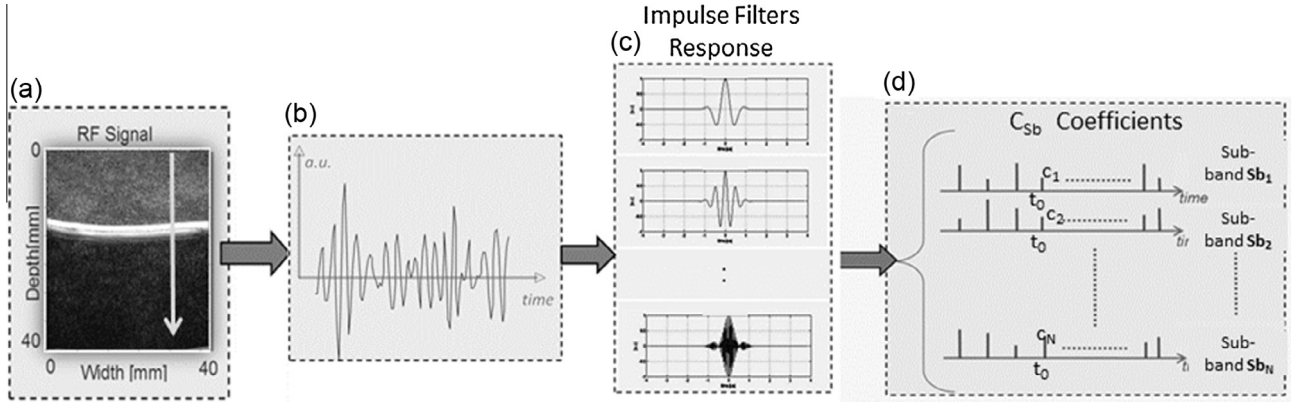

Fig. 2. Sub-Bands decomposition. In (a) the B-Mode of an ultrasonic radiofrequency (RF) frame, related to a transfusion bag of blood is reported. Each track of the RF frame (b) is convolved with N filters (c) and Y tracks of spectral coefficients $c_1, c_2, \ldots, c_N$ are produced, as shown in (d). In (c) some impulse responses of the N filters are illustrated.

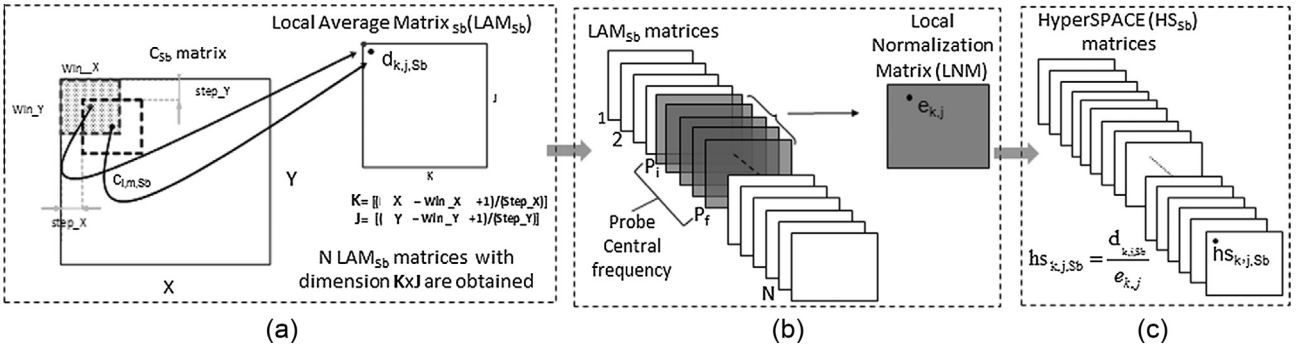

Fig. 3. Local Normalization and Hyperspace Coefficients generation. A local averaging is applied on the absolute values of the N matrices of spectral coefficients (C_{Sb}), in order to obtain Local Average Matrices (LAM_{Sb}) as shown in (a). The Local Normalization Matrix (LNM) is produced by calculating the mean value of the matrices LAM_{Sb} relating to the central frequencies of the employed transducer (b). The HyperSPACE matrices HS_{Sb} are obtained by dividing point to point each matrix LAM_{Sb} by the LNM as illustrated in (c).

$$K = [(X - \text{Win\_}X + 1)/\text{Step\_}X]$$
$$J = [(Y - \text{Win\_}Y + 1)/\text{Step\_}Y] \quad (2)$$

In this work, the window dimensions are Win_X = 6 tracks (1.2 mm), Win_Y = 80 pixels (1.2 mm) and the overlaps Step_X = 2 tracks and Step_Y = 10 pixels.

In (3) the formula that links the coefficients $c_{i,m,\text{Sb}}$ to $d_{k,j,\text{Sb}}$ is as follows:

$$d_{k,j,\text{Sb}} = \frac{1}{\text{Win\_}X \cdot \text{Win\_}Y} \sum_{i=1}^{\text{Win\_}X} \sum_{m=1}^{\text{Win\_}Y} |c_{i,m,\text{Sb}}| \quad (3)$$

The N LAM_{Sb} matrices are therefore constituted by the coefficients $d_{k,j,\text{Sb}}$. In order to assess the magnitude of the ultrasonic signal that locally affects each investigation window considered, the Local Normalization Matrix (LNM) is calculated. In Fig. 3b, it can be seen how the LNM consists of the mean value of the LAM_{Sb} matrices corresponding to the central frequencies of the probe employed. The $e_{k,j}$ coefficients are thus obtained according to the following formula:

$$e_{k,j} = \frac{1}{1 + P_f - P_i} \sum_{\text{Sb}=P_i}^{P_f} d_{k,j,\text{Sb}} \quad (4)$$

where P_i and P_f are the indices related to the initial and final subbands respectively, chosen by considering the central frequency of the transducer used; for the probe LA523 (Esaote S.p.A, Firenze, Italy), P_i = 4 and P_f = 10.

At this point, each of the LAM_{Sb} is divided by the LNM matrix in order to obtain N new locally normalized matrices (HS_{Sb}) constituted by the $hs_{k,j,\text{Sb}}$ coefficients (Fig. 3c) defined by:

$$hs_{k,j,\text{Sb}} = \frac{d_{k,j,\text{Sb}}}{e_{k,j}} \quad (5)$$

These values are the HyperSPACE *hs* coefficients and represent the coordinates of the original samples of the RF frame in the new domain.

At this point, two other phases of the algorithm are carried out, called Training and Classification respectively.

2.3. Training

In the Training phase, Regions of Interest (ROIs) are selected on the B-Mode (Fig. 4a) by the operator. The selection of ROIs is an important operation for ensuring a proper training of the algorithm. In the clinical environment, physicians depending on their experience and based on the echographic appearance draw a closed line around the area to be characterized on the B-Mode. In a laboratory environment, such as in this study, the ROI is selected by taking the echographic appearance and the geometrical, structural and physiological characteristics provided by manufacturers of the test objects into account.

Subsequently, the $hs_{k,j,\text{Sb}}$ coefficients relating to the selected ROIs are analyzed. Fig. 4a shows the B-Mode of a portion of a commercial CIRS model 047 test object (described in detail in Section 3) containing three aggregates with densities differing from the background material they are immersed in. From left to right, the aggregates with +3 dB, +6 dB, and +9 dB are selected respectively on the B-Mode with three different ROIs: ROI 1, ROI 2, and ROI 3. The coefficients of the three ROIs relating to areas with different physical characteristics have different shapes and positions in the hyperspace considered. In order to characterize their distributions, the coefficients are therefore subjected to a clustering process through the iterative algorithm K-means [45]. By considering a partition of data into N clusters, the K-means algorithm is able to define the position of the centroids through an iterative procedure that minimizes the total point-to-centroid distances summed over all N clusters. After this, each cluster is identified by its centroid and by a distance function able to evaluate the degree of separation between clusters.

Fig. 4b shows the different clusters into which the $hs_{k,j,\text{Sb}}$ coefficients related to the ROI 3 are divided. The combination of all the clusters relating to each ROI identifies a hyper volume in the hyperspace characterized by the M centroid and the M by N distances of the clusters it consists of, and which will be called a Configuration (Fig. 4c). This hyper-volume can also be synthetically localized by an average centroid. This is obtained by computing the arithmetic mean of the M centroids belonging to the Configuration.

2.4. Classification

In the Classification phase the $hs_{k,j,\text{Sb}}$ coefficients relating to the whole frame are analyzed and it is determined whether each coefficient belongs to one of the Configurations developed during the Training or not. For each $hs_{k,j,\text{Sb}}$ coefficient, the distance from the centroid of the considered Configuration is calculated in each dimension. If the coefficient is found inside the hyper volume defined by the Configuration, this coefficient will be considered as belonging to the latter. The visualization of the final result is carried out by associating a color code to the pixels of the image related to the $hs_{k,j,\text{Sb}}$ coefficients that belong to each Configuration. This color is then superimposed on the B-Mode grayscale image (Fig. 5). Therefore, if for example three Configurations are present in a frame, the final B-Mode will have three overlapping color codes corresponding to the areas identified by the three Configurations. Fig. 5a illustrates the B-Mode relating to a section of the commercial test object described above. Fig. 5b contains the final results of the Classification. The three Configurations are shown on the B-Mode in red, green and blue, allowing easy identification of the three aggregates with different densities.

3. Materials and methods

The algorithm was tested using calibrated test objects in order to evaluate the ability of the method to detect density variations. Two different test objects with variable densities were used.

The first, as mentioned above, was a commercial CIRS model 047 test object consisting of a background material that simulates the human parenchyma with a series of aggregates with different densities (from −9 dB to +9 dB) and with diameters of 2.4 mm, 4 mm and 6.4 mm, inserted to simulate the presence of cysts. The second was a laboratory test object consisting of a transfusion bag containing human blood immersed in a tank filled with degassed water.

The laboratory tests were performed according to the guidelines of the University of Florence, on human blood provided by a healthy donor who had previously signed an informed consent form. The transfusion bag was filled with different blood concentrations obtained from multiple dilutions with physiological solution. Bags with a capacity of 250 ml and the anticoagulant CPDA (Citrate – Phosphate – Dextrose – Adenine) were used. Through a calibrated and repeatable procedure, 31 different values of Fractional Dilution (FD) were obtained. The FD was defined as follows: $\text{FD} = \text{Vol}_{\text{blood}}/\text{Vol}_{\text{blood+physiological solution}}$, where $\text{Vol}_{\text{blood}}$ is the quantity of blood introduced into the bag and $\text{Vol}_{\text{blood+physiological solution}}$ corresponds to the entire volume of the liquid contained in the same bag. In Fig. 6, the sequence of FD values for the blood samples is reported in a logarithmic diagram.

Fifty RF frames were acquired and processed for each concentration in order to assess the parameter variations as a function

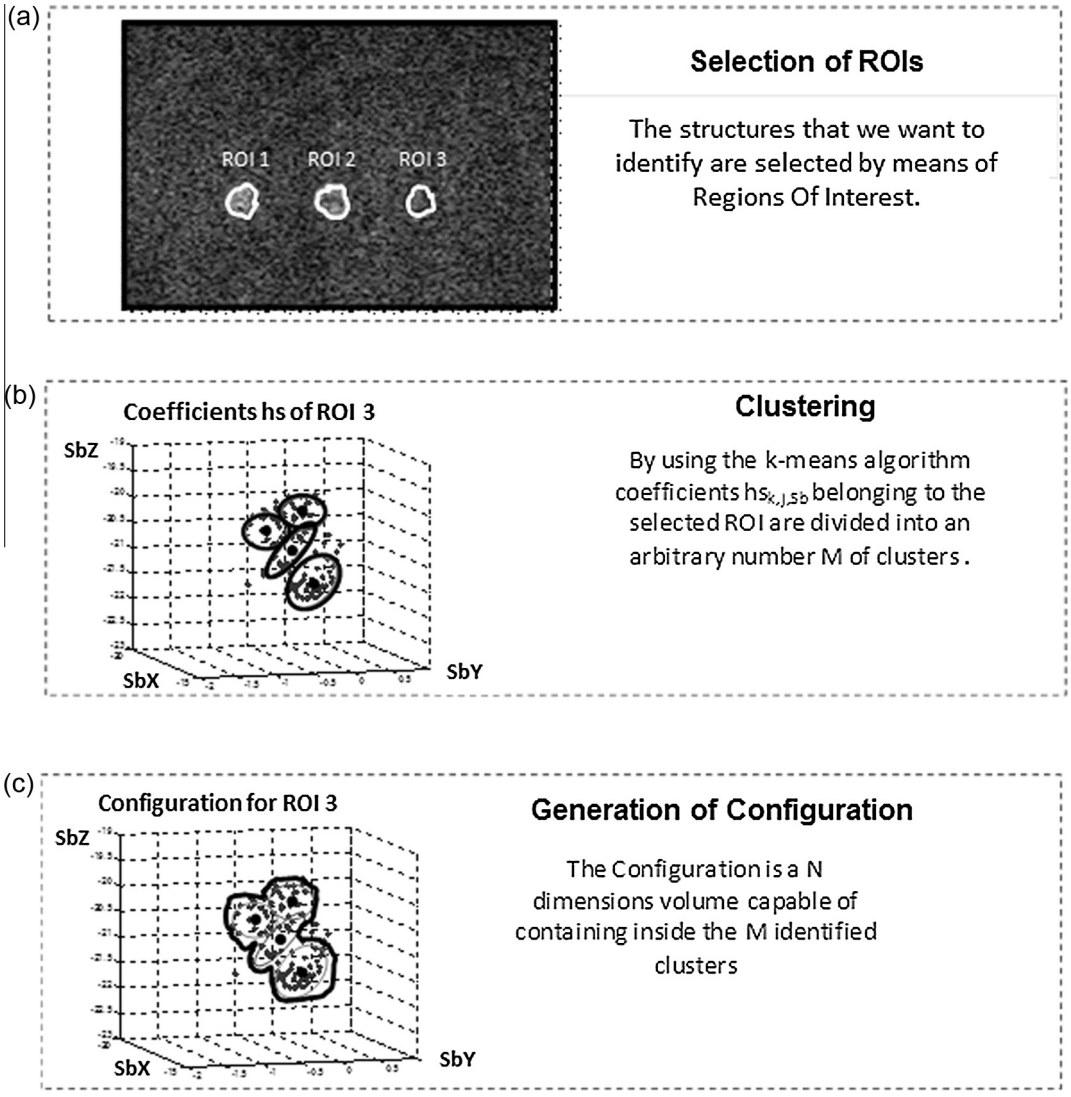

Fig. 4. Training Phase procedure. In (a) Regions Of Interest (ROIs) are identified in the B-Mode image in order to select their *hs* coefficients. The Coefficients are clustered by K-means algorithm and M clusters are generated for each selected ROI, as shown in (a). In (b) the clusters of ROI 3 are considered. The *N*-dimensional volume which collects the M clusters in each ROI is called Configuration, as visualized in (c) for the ROI 3.

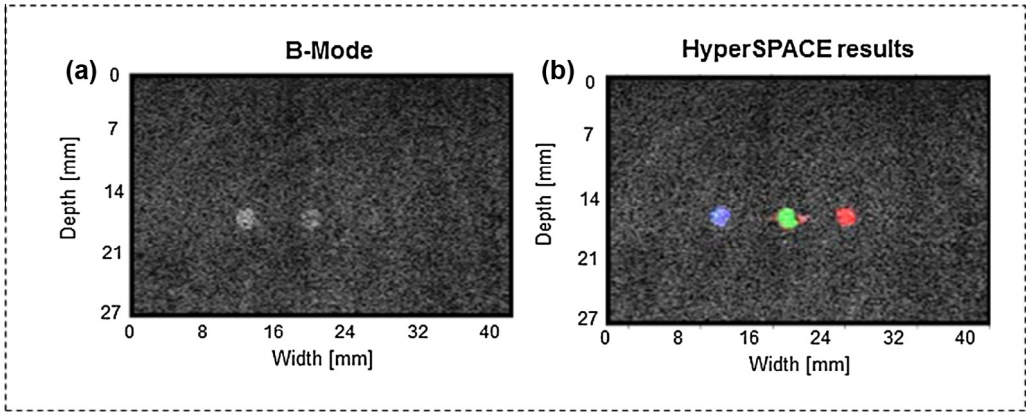

Fig. 5. The Classification phase is performed on the entire analyzed frame in order to detect the presence of the identified Configurations. The figure shows the results obtained on CIRS model 047 (Computerized Imaging Reference Systems, Inc. Norfolk, Virginia 23513 USA) tissue mimicking phantom. The phantom presents cysts with a density differing from the background material. (a) B-Mode image. (b) HyperSPACE results. Each Configuration is associated to a different color. (For interpretation of the references to color in this figure legend, the reader is referred to the web version of this article.)

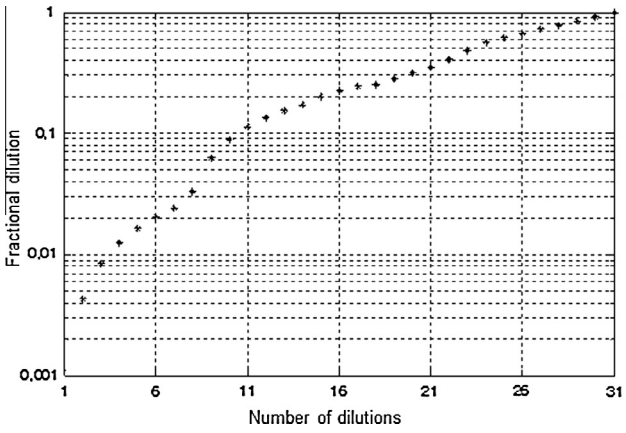

Fig. 6. Values of Fractional Dilutions (FD) of the all blood analyzed samples.

of the FD. This second test object was selected to allow use of a simple and repeatable biological tissue with a variable distribution of scatterers.

In fact, as widely discussed in literature [46–49], blood can be described as a medium [47,48,50] composed of aggregates of red blood cells immersed in plasma. The back-propagated RF signal depends on the concentration of the scatterers and other parameters related to the blood flow. The relation between the frequency of the RF signal, the concentration, and the blood flow parameters has been extensively studied and tested by Cloutier et al. [47,48,51]. Fig. 7 contains the acquisition system. All RF data were collected by means of the FEMMINA (Fast Echographic Multi parameters Multi Image Novel Apparatus) [52,53], a hardware-software platform developed by the Ultrasound and Non-Destructive Testing Laboratory. FEMMINA was used to perform multi-parameter extractions and multi-image data representations starting from the acquired RF signal. For this experiment, FEMMINA was connected to a commercial ultrasound scanner (Mylab 90, Esaote S.p.A, Firenze, Italy), as shown in Fig. 6, which was modified to provide the RF signal output. The ultrasound scanner provides RF beam-formed data sampled at 50 MHz and amplified by the Time Gain Compensation (TGC) module. The data are

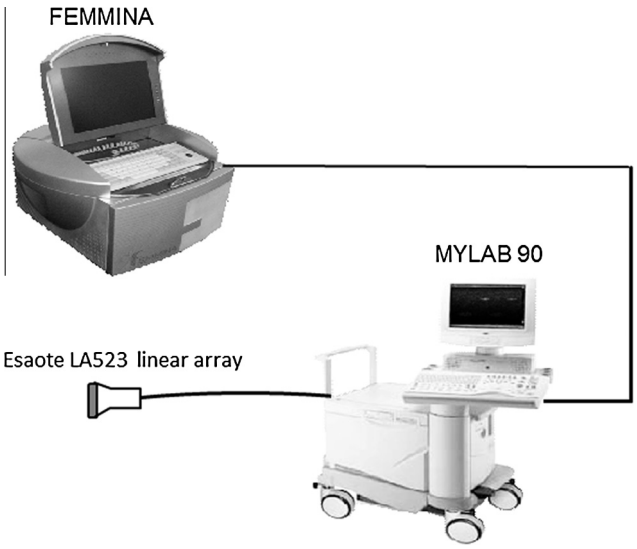

Fig. 7. Acquisition set-up. FEMMINA is connected to the commercial ultrasound scanner Mylab 90 (Esaote S.p.A, Firenze, Italy). The ultrasonic probe is an LA523 linear array (Esaote S.p.A, Firenze, Italy) with a nominal frequency of 7.5 MHz.

transferred to FEMMINA by means of a 1 Gbit/s optical fiber connection. FEMMINA acquires RF data in real time mode at the same frame rate as the scanner. RF data frames can also be stored in the PC memory and then saved on the hard disk to enable an off-line frame-by-frame evaluation. The ultrasonic probe used for this experimentation was an LA523 linear array with a nominal frequency of 7.5 MHz.

4. Experimental results

The algorithm was tested on the CIRS model 047 test object in order to achieve three targets:

1. to evaluate the possibility of differentiating the density of hyper echoic cysts with respect to the background material;
2. to verify whether HyperSPACE is able to reduce attenuation effects, allowing the same Configuration to better identify cysts with the same density at different depths, also thanks to the Local Normalization procedure described in Section 2 and illustrated in Fig. 3;
3. to observe how the Local Normalization makes it possible to detect the same Configuration for the same cyst by varying the ultrasound scanner acquisition settings such as focus depth, transmission power, and total gain.

Before carrying out these experiments, several preliminary tests were performed in order to select the best frequency range subdivision. Different sub-band widths of filters were tested: 3 MHz, 1.5 MHz, 1 MHz and RF frames referring to proximal cysts of the CIRS model 047 were processed. The goodness of the processed images was evaluated in terms of ability to discriminate the density levels and differentiate the cysts from the surroundings. The best compromise was obtained using a 1 MHz frequency sub-band width, as can be observed in Fig. 8 which contains processed HyperSPACE images using 3 MHz, 1.5 MHz and 1 MHz sub-band widths. To achieve the first two objectives, 10 RF frames related to sections not spatially correlated with each other were acquired by moving the probe on the CIRS model 047. The acquired sections contain two rows of cysts with diameters of 2.4 mm and 4 mm respectively at different depths. The acquisition settings were the following: a transmission power of 80%, TGC of 50% at each depth, a total gain of 55%, and a focus position at 20 mm. One of these RF frames was used to train the algorithm and three different ROIs, one for each cyst proximal to the transducer, were selected as illustrated in Fig. 9a. As mentioned above in Section 2, the selection of ROIs is important for ensuring proper training of the algorithm and for this reason we selected the three cysts depending as much as possible on their size. The other 9 sections were used in the Classification phase. The Training phase allowed for identifying the three Configurations, each representing a different degree of density. The Configurations are colored in red, green and blue for the +3 dB, +6 dB, and +9 dB densities respectively. In Fig. 9b and c, it is possible to see how cysts with the same density are characterized by the same Configurations. In particular, it is important to observe how the algorithm detects the presence of the aggregates with a density of +3 dB, which is barely distinguishable from the background material in the B-Mode image. It is even more interesting to note how the cysts with the same density are characterized by the same Configurations, regardless of their different depths, thanks also to the Local Normalization process which reduces the attenuation effects.

In order to test the Configurations by changing the acquisition settings, three other measurement campaigns were performed. For each one, 7 RF frames relating to the same section of the CIRS model 047 were acquired by modifying only one parameter of the

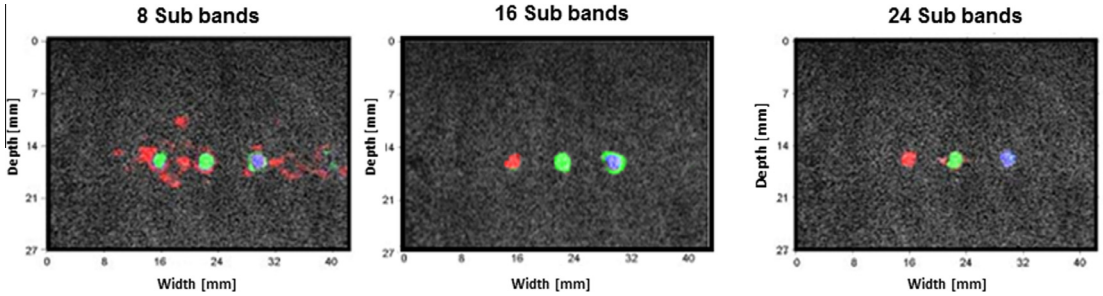

Fig. 8. Three processed HyperSPACE images obtained by decomposing the signal spectrum by means of filters banks with different bandwidths. The first, on the left, is related to a decomposition bank of 8 filters with bandwidth = 3 MHz, the second to a bank of 16 filters with bandwidth = 1.5 MHz and the last to a bank of 24 filters with bandwidth = 1 MHz.

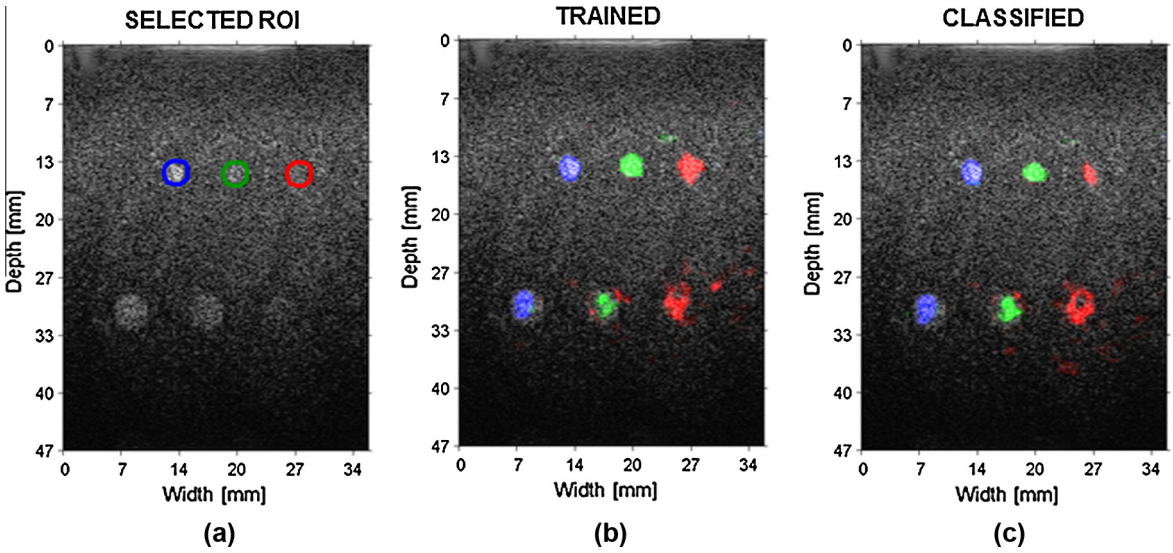

Fig. 9. Training and Classification phase results for CIRS test object. In (a) the selected ROIs are shown. In the Training, only proximal cysts are considered for setting the Configurations. (b) and (c), show the results of the processed frame in Training and Classification, after normalization procedure.

ultrasound scanner at each acquisition. Each of the 7 acquired frames was classified by means of the Configurations identified in the previous training phase, as shown in Fig. 9.

In the first set, the focus depth was changed from a distance of 52 mm to 10 mm. The results relating to the focus depths of 52 mm, 20 mm and 15 mm are shown in Fig. 10a, b and c respectively. In the second set, the parameter considered was the total gain, the dynamics of which were increased from 55% to 90%. The frames with a gain of over 65% were not classified due to the spectral modification effects caused by the saturation of the acquisition system electronics. The results obtained for gains of 55%, 60% and 65% are shown in Fig. 10d, e and f respectively. Gains greater than 65% cause signal saturation and thus the HyperSPACE, which performs a spectral analysis, cannot be applied because it would produce results affected by errors. The incorrect classification of several regions in the images 10e and 10f is a consequence of this phenomenon. In fact, the colors representing the three Configurations are also in the background surrounding the cysts.

The last set was related to the variations in the transmission power parameter within a dynamics range of from 25% to 100%. Figs. 10g–i show the results obtained from the processing of three frames acquired at transmission powers of 80%, 60%, and 40% respectively. As can be seen from all three acquisition campaigns, the algorithm demonstrated good stability due to the three density levels being properly characterized for all the classified frames, irrespective of the variations in the acquisition settings considered.

The algorithm was then tested on the test object consisting of human blood. Fig. 11 shows some of the dilutions with different FDs represented in one of the possible two-dimensional projections of the hyperspace, corresponding to SbX = 3 MHz and Sby = 13 MHz. These two sub-bands have been chosen by way of example. It can be observed how the distribution of the *hs* coefficients is influenced by changing the FD. This induced us to consider the possibility of identifying different concentration levels with specific Configurations. In fact, the clusters of the coefficients labeled FD = 0, which refers to the physiological solution, and FD = 0.005, FD = 0.01, FD = 0.48 and FD = 1.00 corresponding to the human blood, are easily distinguished in this specific two-dimensional projection of the hyperspace.

The use of this test object made it possible to test the algorithm performances. First of all, the capability of producing a Configuration to detect low concentration levels in order to evaluate the electronic sensitivity of the method and moreover the ability to set two different Configurations for acquisitions with FDs very close to each other and with very similar echogenicity in the B-Mode image. For these reasons, FD = 0.01, FD = 0.48 and FD = 0.68 were chosen for training the algorithm. The other frames corresponding to different FD values were only used in the Classification phase. The training produced three Configurations: the first is shown in red relates to FD = 0.68, the second in green to FD = 0.48 and the last in blue to FD = 0.01.

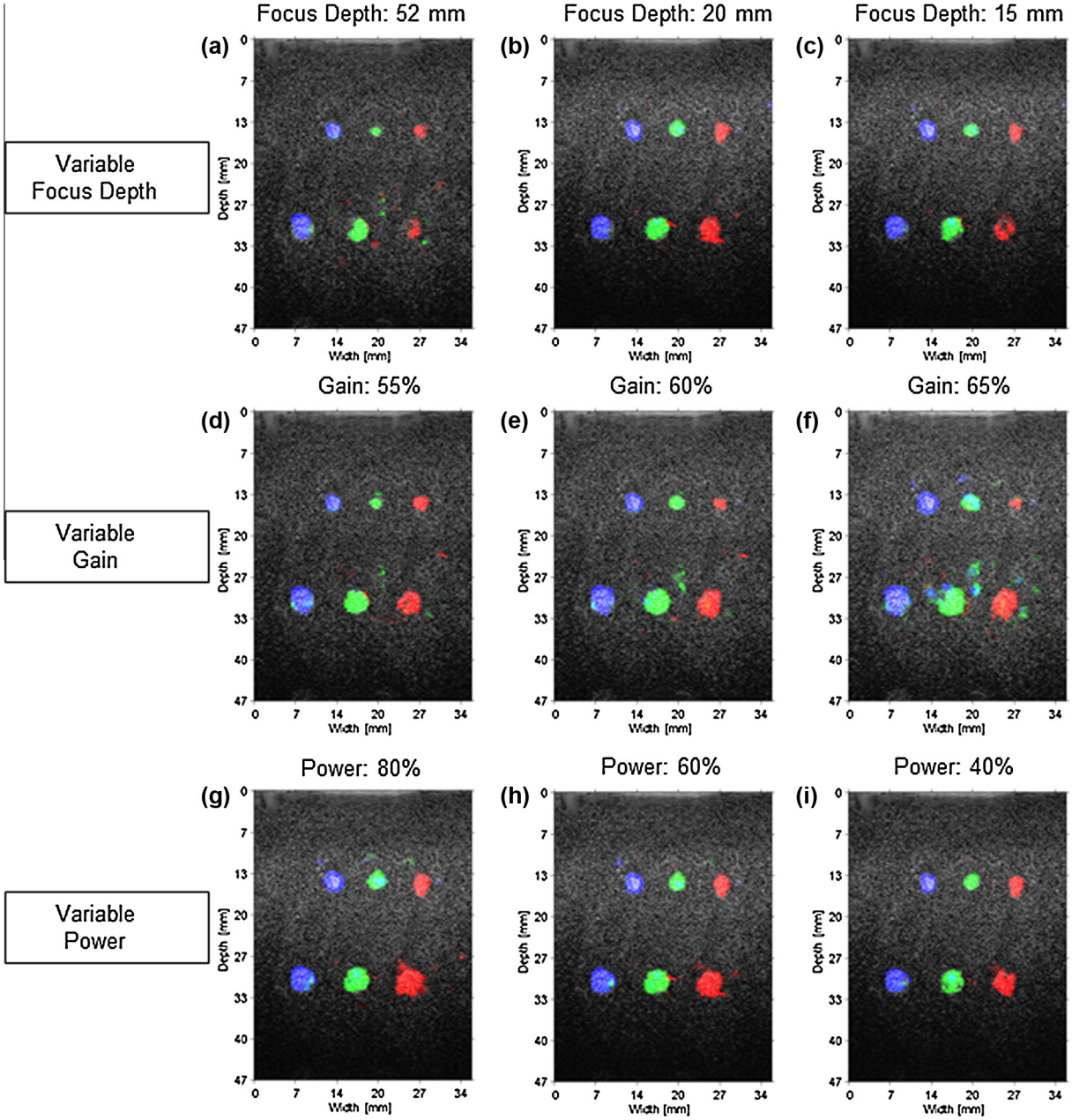

Fig. 10. In (a–c) Classification results obtained at variable focus depths. In (d–f) Classification results obtained for different gains and in (g–i) Classification results obtained for different transmission powers. The analyzed sections contain two rows of cysts with diameters of 2.4 mm (proximal) and 4 mm (at a greater depth).

The average values of the gray levels calculated within a window inside the blood bag for each of the 31 dilutions are reported in Fig. 12. It is worth noting, for example, how the frames with FD = 0.48 and FD = 0.68 show very similar gray-level values. Fig. 13 contains the colored area percentages relating to the three Configurations produced in the training phase. The percentages were estimated on each of the 31 frames, with respect to the entire frame in order to take into account the capability of each Configuration both to characterize only one specific FD value and not to mark areas outside the bag blood, as represented in the B-Mode of Figs. 12 and 14 by the regions below the strong reflection. A good degree of selectivity for the Configurations relating to FD = 0.48 (green), and FD = 0.68 (red) can be observed, as they are minimally superimposed. Fig. 14 contains nine processed images relating to different dilutions. In addition to the three frames used in the training phase, several frames subjected to the classification phase only are also reported. Also in this case, as confirmed by Fig. 13, it is possible to observe how the three Configurations seem to be very selective, i.e. the colored areas on the classified frames are either very small or absent. In Fig. 14 it is evident that the two green and red Configurations, in addition to differing one from the other, do not appear in the frames with dilutions close to FD = 0.48 or FD = 0.68. It can also be observed how the frames used for the training phase are not uniformly colored, due to the inevitable formation of aggregation centers [47].

In order to calculate the specificity (Sp_{FDK}) and sensitivity (Se_{FDK}) of each Configuration, the following expressions were applied [54]:

$$Se_{FDK} = \frac{TP_{FDK}}{TP_{FDK} + FN_{FDK}} \qquad Sp_{FDK} = \frac{TN_{FDK}}{TN_{FDK} + FP_{FDK}} \tag{6}$$

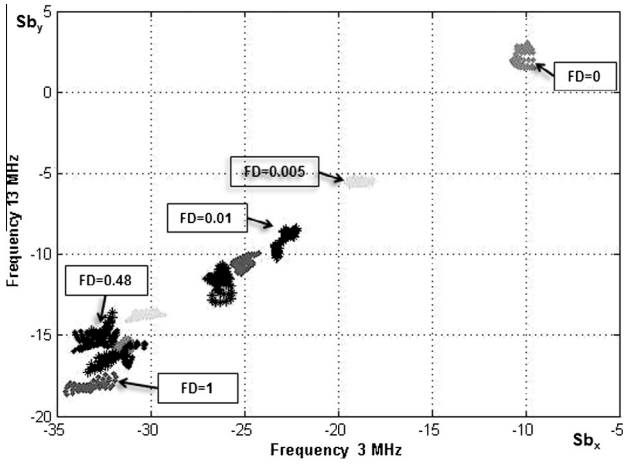

Fig. 11. Example of coefficients *hs* at different FD values is shown in a two-dimensional projection of the *N* dimension hyperspace. The choice of these sub-bands in the figure is only to give an example. It is worth noting that different clusters correspond to different FD values.

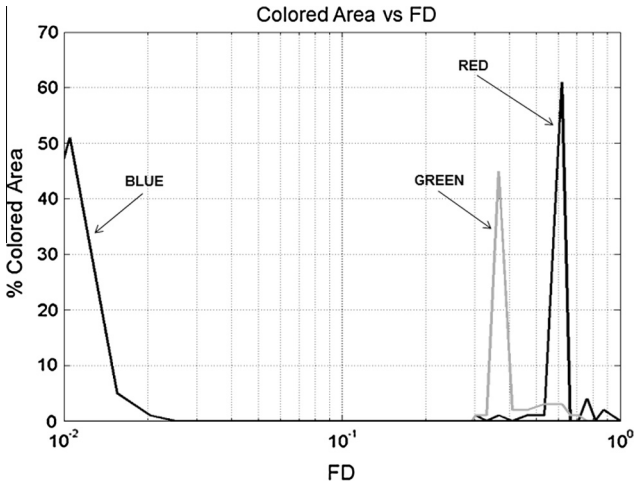

Fig. 13. Percentage of Colored Area calculated on every frame with different FD depending on the FD values. The percentage is calculated for the entire frame. It can be noted how the three colors have very low superimpositions for different FD values and are very specific for the FD selected for the training.

where

TP_{FDK}: area of regions into blood bags with FD = *FDK* truly stained by Configuration for FD = *FDK*;

FN_{FDK}: area of regions into blood bags with FD = *FDK* falsely not stained by Configurations for FD = *FDK*;

FP_{FDK}: area of regions into blood bags with FD ≠ *FDK* falsely stained by Configuration for FD = *FDK*;

TN_{FDK}: area of regions into blood bags with FD ≠ *FDK* truly not stained by Configurations for FD = *FDK*.

Estimated values for the defined Configurations are reported in Table 1.

The obtained values are due to the choice of having trained the method favoring the specificity with respect to sensitivity. Actually, in many cases the clinical diagnosis is concerned, not only to detect the presence of disease, but especially to differentiate its nature from other types of pathologies with high level of safety. Another consideration needs to be made about Se_{FDK}, that, according to the definition of TP_{FDK} and FN_{FDK}, resulted to be affected by the non homogeneous FD distribution into the blood bags, as said above.

Moreover, the minimum FD level detectable by the BLUE Configuration was FD = 0.01 and represent the electronic sensitivity of HyperSPACE method. In fact, it was decided to set a Configuration for FD = 0.005, however, FD = 0 was also marked in the Classification, demonstrating that noise and no blood was detected.

It must be pointed out that to assess the stability of a processing method, it is necessary to evaluate its performance as a function of the signal-to-noise (SNR) ratio. In order to achieve this for the HyperSPACE, the acquisition with FD equal to 1 is considered. Moreover, an acquisition was performed with the transducer immersed in water with identical parameters to those used in the acquisition with FD = 1. Different values of synthetic coherent noise created in the Matlab environment (MathWorks, Natick, Massachusetts, USA) were added to this acquisition to obtain 32 different frames with increasing noise. The synthetic noise was filtered by the frequency response of the probe used. On each of these frames, the same ROI was selected in the focalized region and the noise was calculated for the 32 different values of the added synthetic noise, according to the formula:

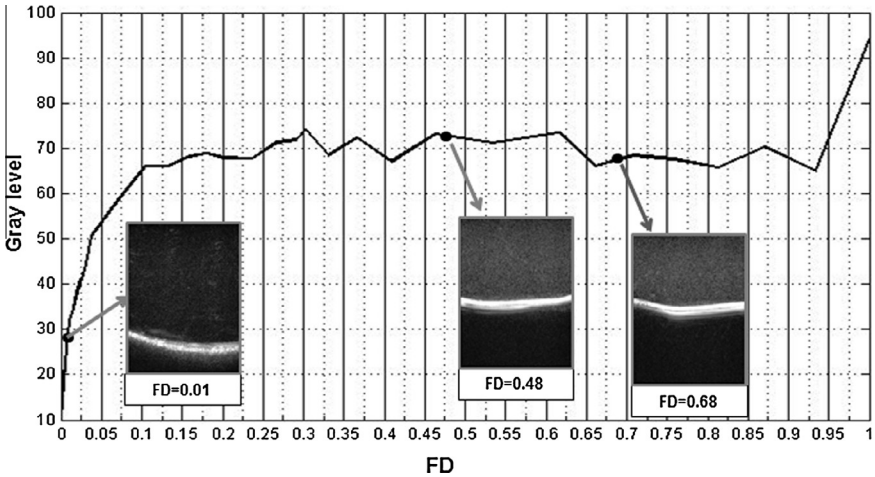

Fig. 12. Gray level mean value calculated on the B-Mode images, in relation to different FD values. For FD from 0.25 up to 0.9, the gray level mean has small fluctuations and therefore it is very difficult to distinguish the different dilution levels through the analysis of the B-Mode images.

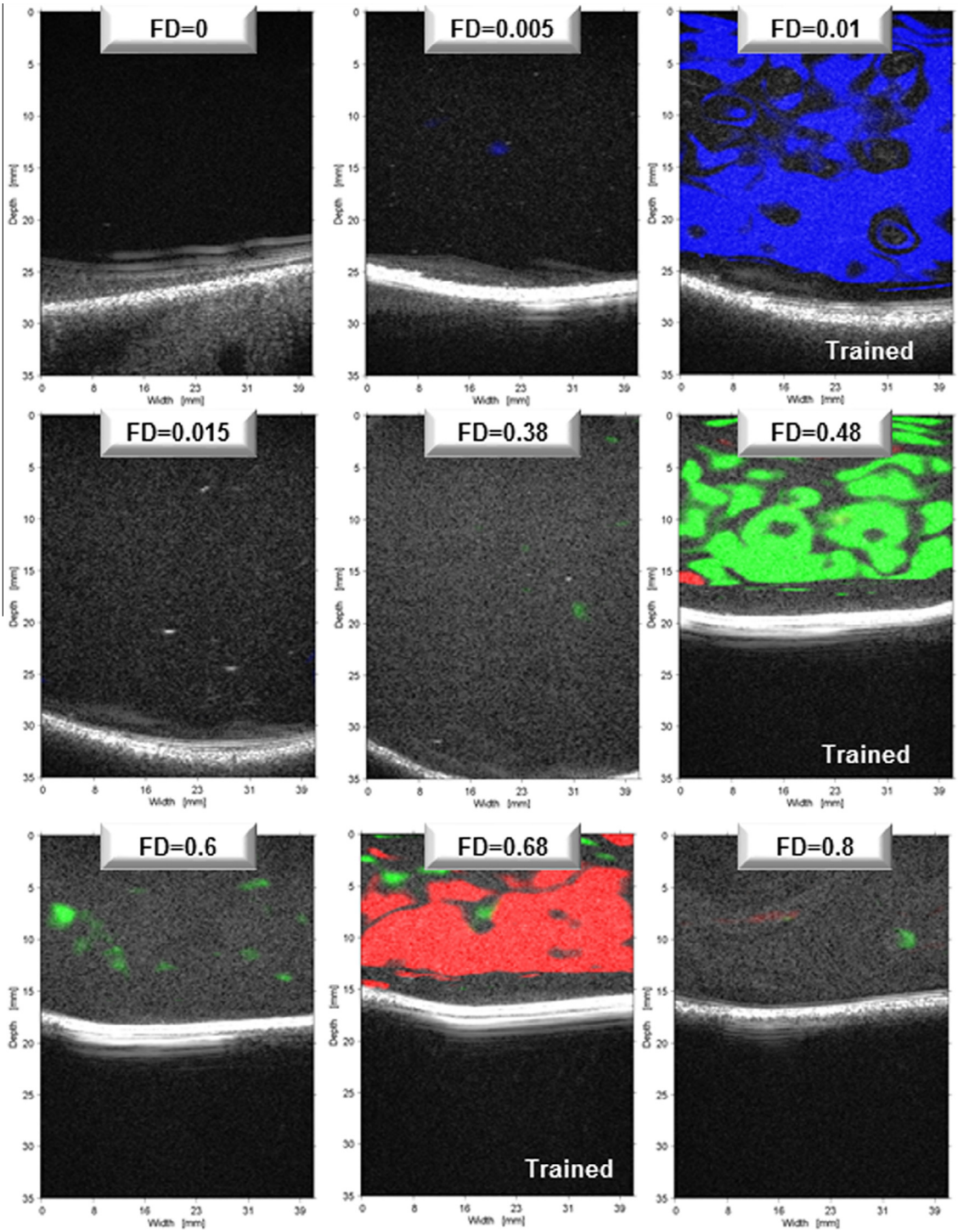

Fig. 14. Results obtained on blood bags with different FD values are reported. Three Configurations have been set: the blue for FD = 0.01, the green for FD = 0.48 and the red for FD = 0.68. They are very specific, that is, they mainly characterize the frames of the blood bags with these FD specific values of FD and only very small colored spots are visible for the other FD values. The algorithm also shows a high electronic sensitivity, in fact, it is capable of detecting the presence of blood for very small concentrations (FD = 0.01). (For interpretation of the references to color in this figure legend, the reader is referred to the web version of this article.)

Table 1
Values of specificity (Sp_{FDK}) and sensitivity (Se_{FDK}) of each Configuration.

Configuration	Fractional dilution (FDK)	Se_{FDK} (%)	Sp_{FDK} (%)
Red	0.68	71.0	99.6
Green	0.48	50.2	99.6
Blue	0.01	44.5	99.8

$$\mathrm{SNR} = 10 * \log 10 \frac{((Signal + Electronic\ Noise)_{FD1})^2}{(Electronic\ Noise_{WATER} + Synthetic\ Noise)^2} \quad (7)$$

where

$(Signal + Electronic\ Noise)_{FD}$: acquired signal for FD = 1;
$Electronic\ Noise_{WATER}$: acquired signal in water.

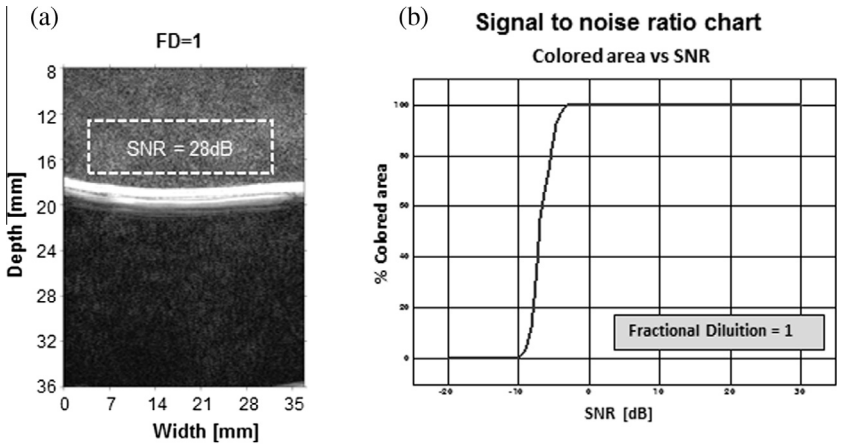

Fig. 15. The acquisition with FD equal to 1.0 was gradually added with synthetic additive noise. A ROI was selected in all the processed frames and its percentage of colored area was evaluated. (a) Selected ROI. (b) Resulting curve at different levels of SNR.

Fig. 15a contains the frame for FD = 1 with the selected ROI. In this region the SNR is equal to 28 dB, as derived from formula (7) with no added synthetic noise. The FD = 1 RF frame without any synthetic noise was processed in order to define a specific Configuration relating to the corresponding concentration level. After which, each frame corresponding to a different value of SNR was processed. The consistency of the colored-area Configuration was tested by evaluating the area percentage with respect to the entire ROI area for each different level of added noise.

Fig. 15b contains the graph representing the percentages of covered area as a function of SNR.

It can be observed how the percentage of the colored area remains unchanged at 100% of the ROI until the SNR level reaches 3 dB. When the noise increases further, the percentage of colored area decreases in an almost linear manner until finally disappearing when the SNR level is equal to −10 dB.

5. Discussion

Over the last three decades, researchers using QUS techniques have demonstrated that the interaction between the ultrasonic signal and the investigated structures gives rise to alterations in the RF amplitude and frequency. As already affirmed by the authors in previous publications, the HyperSPACE algorithm extracts spectral features correlated to the structures of the investigated medium. More specifically, the medium density was analyzed in this work by using two stable and repeatable test objects. The use of these kinds of test objects allowed for the standardization and repeatability of the procedures. With the commercial CIRS model 047, it was possible to change the analyzed parameter with different resolutions through different dilution levels in the blood bags, as well as ensure the replicability of results.

The study of spectral parameters enables detection of RF signal alterations due to the organizational and structural characteristics. The analysis of the results highlights how spectral parameters extracted via use of the proposed method provide a significant increase in information regarding the investigated structure in comparison with that supplied by the B-Mode. For example, from the analysis of the B-Mode of the CIRS phantom in Fig. 5, the +3 dB cysts are difficult to distinguish; in addition, from the observation of the B-Modes related to blood bags as shown in Fig. 12, it is very difficult to discriminate the levels of dilution from FD = 0.25 up to FD = 0.9. The HyperSPACE exploits a different type of processing that analyzes the signal in a new spectral domain in which it appears possible to obtain more information about the structure and the organization of the investigated medium. In fact, during the Training phase, the proposed method is able to characterize the three cysts with three different densities by providing a Configuration for each density value. In the Classification, the cysts are correctly detected by the same Configurations without marking external areas even in uncorrelated sections or for different acquisition settings of the ultrasound scanner, as illustrated in Fig. 10.

In addition, the analysis of blood bags has demonstrated that it is possible to define a Configuration for every FD level with high specificity. The clusters referring to different FD values in fact have different shapes and positions in the hyperspace as confirmed in Fig. 11. In the present experimentation, only three Configurations were set and discussed for the sake of simplicity.

Indeed, the "local normalization" of the coefficients is a specific and innovative characteristic of the proposed method as it enables normalization of the spectral contents of each "local" portion of the investigated medium from the energy of the ultrasonic wave that has actually insonified it.

The results obtained from the analysis of different SNR levels have demonstrated the stability of the colored area, confirming the validity of the selected Configuration. By gradually inserting the synthetic additive noise, the percentage of the colored area remains unchanged at 100% of the ROI until the SNR level reaches 3 dB. When the noise further increases, the percentage of colored area decreases in an almost linear manner until finally disappearing when the level of SNR is equal to −10 dB. This fact is very encouraging for future applications in tissue characterization where low SNR conditions occur as in the case of micro vascularization detection.

6. Conclusion

This paper presents the fundamental stages and properties of the HyperSPACE analysis method. The algorithm has already been applied to *in vivo* experimentation on breast tissue differentiation where it has achieved significant results. Based on RF ultrasonic signal processing, it works in a *N*-dimensional spectral domain. In the Training phase, the method characterizes areas at different densities by selecting ROIs with different structural organizations and producing Configurations. In the Classification phase, where the entire frame is processed, the aim of the method is to detect the regions of the investigated medium the hyperspace *hs* coefficients of which belong to previously identified Configurations. Regions with the same density are correctly detected by the specific Configurations without marking any other portions. The ability

of the HyperSPACE to differentiate density levels has been evaluated via use of two stable and repeatable test objects.

The two specific characteristics of the method are the identification of a new spectral domain, the dimension of which depends on the number of sub-bands into which the RF signal is decomposed, and the "local normalization" that allows for analyzing variations in the back-propagated signal compared to the actual ultrasonic signal present in the investigated portion of the medium. Moreover, the HyperSPACE has demonstrated great robustness with respect to the signal-to-noise ratio. In fact, the method was able to recognize the Configuration with a 50% covered area at a SNR equal to −7 dB.

Acknowledgment

This work was promoted and funded by the Regione Toscana within the FORTE research project of the operational regional program Por Creo Fesr 2007–2013.

References

[1] G. Ghoshal, J. Mamou, M.L. Oelze, State of art methods for estimating backscater coefficient, in: J. Mamou, M.L. Oelze (Eds.), Quantitative Ultrasound in Soft Tissues, Springer, 2013, pp. 3–20 (Chapter 2).
[2] E.J. Feleppa, M.M. Yaremko, Ultrasonic tissue characterization for diagnosis and monitoring, IEEE Eng. Med. Biol. 6 (4) (1987) 18–26.
[3] E.J. Feleppa, L. Liu, A. Kalisz, M.C. Shao, N. Fleshner, V. Reuter, W.R. Fair, Ultrasonic spectral-parameter imaging of the prostate, Int. J. Imag. Syst. Technol. 8 (1997) 11–25.
[4] E.J. Feleppa, J.A. Ketterling, A. Kalisz, S. Urban, C.R. Porter, J.W. Gillespie, P.B. Schiff, R.D. Ennis, C.S. Wuu, W.R. Fair, Advanced ultrasonic tissue typing, and imaging based on radio-frequency spectrum analysis, and neural-network classification for guidance of therapy, and biopsy procedures, in: Proc CARS, vol. 15, 2001, pp. 333–337.
[5] R. Jurkonis, A. Janušauskas, V. Marozas, D. Jegelevičius, S. Daukantas, M. Patašius, A. Paunksnis, A. Lukoševičius, Algorithms and results of eye tissues differentiation based on RF ultrasound, Sci. World J. (2012) 1–6.
[6] M. Moradi, P. Abolmaesumi, P. Mousavi, Tissue typing using ultrasound RF time series: experiments with animal tissue samples, Med. Phys. 37 (2010) 4401–4413.
[7] G. Schmitz, H. Ermert, T. Senge, Tissue-characterization of the prostate using radio frequency ultrasonic signals, IEEE Trans. Ultrason., Ferroelectr., Freq. Control 46 (1999) 126–138.
[8] R.F. Wagner, M.F. Insana, D.G. Brown, Statistical properties of radio-frequency and envelope-detected signals with applications to medical ultrasound, J. Opt. Soc. Am. A 4 (5) (1987) 910–922.
[9] F.L. Lizzi, M. Astor, E.J. Feleppa, M. Shao, A. Kalisz, Statistical frame work for ultrasonic spectral parameter imaging, Ultras. Med. Biol. 23 (1997) 1371–1382.
[10] M. Pereyra, H. Batatia, Modeling ultrasound echoes in skin tissues using symmetric a – stable process, IEEE Trans. Ultrason., Ferroelectr., Freq. Control. 59 (1) (2012) 60–72.
[11] G. Ghoshal, M.L. Oelze, W.D. O'Brien Jr., Quantitative ultrasound history and successes, in: J. Mamou, M.L. Oelze (Eds.), Quantitative Ultrasound in Soft Tissues, Springer, 2013, pp. 21–42.
[12] J. Mamouy, E. Saegusa-Beecroft, A. Coronzx, M.L. Oelze, L.Yamaguchi, M. Hata, E. Yanagihara, J. Machi, P. Laugierzx, E.J. Feleppay, F.L Lizzi, Spatial-resolution optimization of 3D high-frequency quantitative ultrasound methods to detect metastatic regions in human lymph nodes, in: IEEE Int. Ultrason. Symp., 2013, pp. 1216–1219.
[13] H. Tadayyon, A. Sadeghi-Naini, G.J. Czarnota, Noninvasive characterization of locally advanced breast cancer using textural analysis of quantitative ultrasound parametric images, Translational Oncol. 7 (2014) 759–767.
[14] M. Aboofazeli, P. Abolmaesumi, G. Fichtinger, P. Mousavi, Tissue characterization using multiscale products of wavelet transform of ultrasound radio frequency echoes, in: Proc. of 31st Ann. Int. Conf. of the IEEE EMBS, Minneapolis, Minnesota, USA, September 2–6, 2009, pp. 479–482.
[15] K.D. Donohue, L. Huang, T. Burks, F. Forsberg, C.W. Piccoli, Tissue classification with generalized spectrum parameters, Ultras. Med. Biol. 27 (2001) 1505–1514.
[16] G. Georgiou, F.S. Cohen, Tissue characterization using the continuous wavelet transform Part I: decomposition method, IEEE Trans. Ultrason., Ferroelectr., Freq. Control 48 (2) (2001) 355–363.
[17] P. Guillemain, R. Kronland-Martinet, Characterization of acoustic signals through continuous linear time-frequency representations, in: Proc. IEEE, vol. 84, no. 4, 1996, pp. 561–587.
[18] F.L. Lizzi, M.A. Laviola, D.J. Coleman, Tissue signature characterization utilizing frequency domain analysis, in: Proc. IEEE Ultrasonics Symp., 1976, pp. 714–719.
[19] F.L. Lizzi, M. Greenebaum, E.J. Feleppa, M. Elbaum, D.J. Coleman, Theoretical framework for spectrum analysis in ultrasonic tissue characterization, J. Acoust. Soc. Am. 73 (4) (1983) 1366–1373.
[20] F.L. Lizzi, E.J. Feleppa, S.K. Alam, C.X. Deng, Ultrasonic spectrum analysis for tissue evaluation, Pattern Recogn. Lett. 24 (2003) 637–658.
[21] U. Scheipers, H. Ermert, H.J. Sommerfeld, M. Garcia-Schürmann, T. Senge, S. Philippou, Ultrasonic multifeature tissue characterization for prostate diagnostics, Ultras. Med. Biol. 29 (8) (2003) 1137–1149.
[22] G. Schmitz, H. Ermert, T. Senge, Tissue characterization of the prostate using Kohonen-maps, in: Proc. IEEE Ultrasonics Symp., vol. 2, 1994, pp. 1487–1490.
[23] J. Wang, C. Kang, X. Liu, T. Li, Y. Wang, T. Feng, Z. Li, N. Xue, K. Shi, Clinical value of radiofrequency ultrasonic local estimators in classifying breast lesions, J. Ultras. Med. 32 (1) (2013) 83–92.
[24] J. Wang, C. Kang, T. Feng, J. Xue, K. Shi, T. Li, X. Liu, Y. Wang, Effect of instrument settings on liquid-containing lesion images characterized by radiofrequency ultrasound local estimators, Z. Med. Phys. 23 (2) (2013) 94–101.
[25] J. Wang, C. Kang, T. Feng, J. Xue, K. Shi, T. Li, X. Liu, Y. Wang, Effects of instrument settings on radiofrequency ultrasound local estimator images: a preliminary study in a gallbladder model, Mol. Med. Rep. 8 (4) (2013) 995–998.
[26] E. Biagi, L. Masotti, L. Breschi, M. Calzolai, L. Capineri, S. Granchi, M. Scabia, Radiofrequency real time processing: ultrasonic spectral images and vector doppler investigation, in: Proc. 25th Int. Symp. Acoust. Imaging, vol. 25, 2000, pp. 419–426.
[27] L. Masotti, E. Biagi, A. Acquafresca, L. Breschi, M. Calzolai, R. Facchini, A. Giombetti, S. Granchi, A. Ricci, M. Scabia, Ultrasonic images of tissue local power spectrum by means of wavelet packets for prostate cancer detection, in: Proc. 26th Int. Symp. Acoust. Imaging, vol. 26, 2002, pp. 97–104.
[28] E. Biagi, S. Granchi, L. Breschi, E. Magrini, F. Di Lorenzo, L. Masotti, Tissue differentiation based on radiofrequency echographic signal local spectral content, in: Proc. IEEE Ultrasonics Symp., Honolulu, USA Oct. 5–8, 2003, pp. 1030–1033.
[29] E. Biagi, L. Breschi, S. Granchi, L. Masotti, Metodo e dispositivo perfezionati per l'analisi spettrale locale di un segnale ecografico, Italian Patent FI2003A000254, Oct. 8, 2003.
[30] L. Masotti, E. Biagi, S. Granchi, L. Breschi, Method and Device for Spectral Analysis of an Echographic Signal, US Patent, Pub. No. US 2003/0167003 A1, Sep. 4, 2003.
[31] L. Masotti, E. Biagi, L. Breschi, S. Granchi, F. Di Lorenzo, E. Magrini, Tissue differentiation based on radiofrequency echographic signal local spectral content (RULES: Radiofrequency Ultrasonic Local Estimator), in: Proc. IEEE Ultrasonics Symp., 2003, pp. 1030–1033.
[32] L. Masotti, E. Biagi, A. Acquafresca, L. Breschi, F. Di Lorenzo, S. Granchi, R. Facchini, E. Magrini, F. Rindi, M. Scabia, G. Torricelli, Real time images of local ultrasonic spectral parameters for tissue differentiation through Wavelet Transform, in: Proc. 27th Int. Symp. Acoust. Imaging, vol. 27, 2003, pp. 485–491.
[33] L. Masotti, E. Biagi, S. Granchi, L. Breschi, E. Magrini, F. Di Lorenzo, Clinical test of RULES (RULES: radiofrequency ultrasonic local estimators), in: Proc. IEEE Ultrasonics Symp., vol. 3, 2004, pp. 2173–2176.
[34] L. Masotti, E. Biagi, S. Granchi, A. Luddi, L. Breschi, R. Facchini, Carotid plaque tissue differentiation based on radiofrequency echographic signal local spectral content (RULES: Radiofrequency Ultrasonic Local Estimators), in: P. IEEE Int. Symp. on Biomed. Imaging, 2008, pp. 1051–1054.
[35] S. Granchi, E. Vannacci, E. Biagi, L. Masotti, Differentiation of breast lesions by use of HyperSPACE: hyper-spectral analysis for characterization in echography, Ultrasound Med. Biol 41 (7) (2015) 1967–1980.
[36] E. Biagi, S. Granchi, E. Vannacci, L. Lucarini, L. Masotti, Tissue characterization in echographic spectral hyperspace: breast pathologies differentiation, in: Proc. IEEE Ultrason. Symp., San Diego, California, 2010, pp. 1388–1391.
[37] E. Biagi, S. Granchi, E. Vannacci, L. Masotti, A. Martegani, First multicenter experience in differentiation of breast lesions by HyperSPACE SPectral analysis in echography, in: presented at 97th Scientific Assembly and Annual Meeting of RSNA, Chicago, 27 Nov.– 2 Dec. 2011.
[38] N.D. Kim, V. Amin, D. Wilson, G. Rouse, S. Udpa, Texture analysis using multiresolution analysis for ultrasound tissue characterization, in: Rev. of Progress in Quantitative Nondestructive Evaluation, vol. 16, 1997, pp. 1351–1358.
[39] A. Materka, M. Strzelecki, Texture analysis methods – a review, Report of Technical University of Lodz, Institute of Electronics, COST B11 Report, Brussels, 1-33, 1998, available at: <http://www.eletel.p.lodz.pl/programy/cost/pdf_1.pdf>.
[40] P.D. Wankhade, A review on aspects of texture analysis of images, Int. J Appl. Innov. Eng. Manage. (IJAIEM) 3 (10) (2014) 229–232.
[41] H. Chen, M.J. Zuo, X. Wang, M.R. Hoseini, An adaptive Morlet wavelet filter for time-of-flight estimation in ultrasonic damage assessment, Measurement 43 (4) (2010) 570–585.
[42] J. Choi, J.W. Hong, Characterization of wavelet coefficients for ultrasonic signals, J. Appl. Phys. 107 (114909) (2010) 2–6.
[43] S.S. Osofsky, Calculation of transient sinusoidal signal amplitudes using the Morlet wavelet, IEEE Trans. Signal Process. 47 (12) (1999) 3426–3428.
[44] L. Yue, L. Zhang, Application of Morlet wavelet filter to frequency response functions preprocessing, in: Proc. SEM IMAC-XXII: Conference & Exposition on Structural Dynamics, 2004.

[45] J.B. MacQueen, Some methods for classification and analysis of multivariate observations, in: Proc. of 5-th Berkeley Symposium on Mathematical Statistics and Probability, University of California Press, Berkeley, 2015, pp. 281–297.
[46] G. Cloutier, Z. Qin, Ultrasound backscattering from non-aggregating and aggregating erythrocytes – a review, Biorheology 34 (6) (1997) 443–470.
[47] I. Fontaine, M. Bertrand, G. Cloutier, A system-based approach to modeling the ultrasound signal backscattered by red blood cells, Biophys. J. 77 (1999) 2387–2399.
[48] E. Franceschini, B. Metzger, G. Cloutier, Forward problem study of an effective medium model for ultrasound blood characterization, IEEE Trans. Ultrason. Ferroelectr. Freq. Control 58 (12) (2011) 2668–2679.
[49] E. Franceschini, R. Guillermin, Experimental assessment of four ultrasound scattering models for characterizing concentrated tissue-mimicking phantoms, J. Acoust. Soc. Am. 132 (6) (2012) 3737–3747.
[50] E. Franceschini, G. Cloutier, Modeling of ultrasound backscattering by aggregating red blood cells, in: J. Mamou, M.L. Oelze (Eds.), Quantitative Ultrasound in Soft Tissues, Springer, 2013, pp. 117–146 (Chapter 6).
[51] R.K. Saha, M.C. Koliosa, A simulation study on photoacoustic signals from red blood cells, J. Acoust. Soc. Am. 129 (5) (2011) 2935–2943.
[52] E. Biagi, M. Calzolai, L. Capineri, S. Granchi, L. Masotti, M. Scabia, FEMMINA: a fast echographic multi parameter multi imaging novel apparatus, in: Proc. IEEE Ultrasonics Symp., 1999, pp. 739–748.
[53] M. Scabia, E. Biagi, L. Masotti, Hardware and software platform for real-time processing and visualization of echographic radiofrequency signals, IEEE Trans. Ultrason. Ferroelectr. Freq. Control 49 (2002) 1444–1452.
[54] T. Fawcett, An introduction to ROC analysis, Pattern Recogn. Lett. 27 (8) (2006) 861–874.